MATERIALS SCIENCE

Terapascal static pressure generation with ultrahigh yield strength nanodiamond

10.1126/sciadv.1600341

Natalia Dubrovinskaia,[1]*† Leonid Dubrovinsky,[2]† Natalia A. Solopova,[1,2] Artem Abakumov,[3]‡ Stuart Turner,[3] Michael Hanfland,[4] Elena Bykova,[2] Maxim Bykov,[2] Clemens Prescher,[5] Vitali B. Prakapenka,[5] Sylvain Petitgirard,[2] Irina Chuvashova,[1,2] Biliana Gasharova,[6] Yves-Laurent Mathis,[7] Petr Ershov,[8] Irina Snigireva,[4] Anatoly Snigirev[4,8]

Studies of materials' properties at high and ultrahigh pressures lead to discoveries of unique physical and chemical phenomena and a deeper understanding of matter. In high-pressure research, an achievable static pressure limit is imposed by the strength of available strong materials and design of high-pressure devices. Using a high-pressure and high-temperature technique, we synthesized optically transparent microballs of bulk nanocrystalline diamond, which were found to have an exceptional yield strength (~460 GPa at a confining pressure of ~70 GPa) due to the unique microstructure of bulk nanocrystalline diamond. We used the nanodiamond balls in a double-stage diamond anvil cell high-pressure device that allowed us to generate static pressures beyond 1 TPa, as demonstrated by synchrotron x-ray diffraction. Outstanding mechanical properties (strain-dependent elasticity, very high hardness, and unprecedented yield strength) make the nanodiamond balls a unique device for ultrahigh static pressure generation. Structurally isotropic, homogeneous, and made of a low-Z material, they are promising in the field of x-ray optical applications.

INTRODUCTION

The behavior of matter at extreme conditions is fascinating and has attracted the attention of a broad research community for decades. Compression gives rise to a qualitative modification of properties of matter, inducing structural and magnetic phase transitions, including formation of atomic solid hydrogen (*1*), or superconductivity, especially at unprecedented high temperatures (*2*), and formation of new "super" states of matter (*3*). Extreme stresses affect the electronic structure of materials. Insulator-to-metal transitions (*4*) and the topological changes of the Fermi surface for valence electrons, which are known as electronic topological transitions, represent well-known examples of the electronic transitions. A novel type of electronic transitions, so-called core-level crossing transition, was recently reported in osmium compressed to greater than 770 GPa (*5*). Achieving higher and higher pressures opens new horizons for a deeper understanding of matter and modeling the interior of giant and extraterrestrial (super-Earth) planets (*6*) but requires a permanent development of ultrahigh-pressure generation technology: both high-pressure devices and materials used in these devices that could sustain extraordinary pressures.

Bulk nanostructured materials often have physical properties overcoming those of their single-crystal or polycrystalline counterparts (*7*). The strongest presently known materials, bulk nano-polycrystalline diamond (NPD) (*8*) and nanocrystalline diamond (NCD) (*9*), were first purposely synthesized using the high pressure–high temperature (HPHT) technique from graphite and C_{60}, respectively, about a decade ago. NPD and NCD have a different microstructure: NPD contains both nano-sized and submicrometer-sized grains, whereas NCD consists only of nanoparticles smaller than 50 nm. By now, synthesis of NPDs and NCDs has been realized from various precursors (graphite, onion carbon, fullerite, glassy carbon, and others) (*10*–*13*). Investigations of NPD and NCD have revealed their extreme hardness, thermal stability, fracture toughness, and wear resistance (*8*, *11*, *14*–*16*) compared to single-crystal diamond. These extraordinary properties have stimulated further scientific and industrial interest in HPHT bulk nanodiamonds. For instance, NPD is now commercially produced from graphite by Sumitomo Electric Ltd. for use in hard tools and as anvils in multianvil apparatuses and diamond anvil cells (DAC) (*17*). Recently, NCD was synthesized from glassy carbon in the form of translucent microballs of 20 to 50 μm in diameter (*13*). They were used as secondary anvils in double-stage DAC (ds-DAC) experiments to generate static pressures exceeding 600 GPa (*13*). Since then, other groups have tried to use the ds-DAC technique (*18*–*20*), however, employing single-crystal diamond, NPD, or chemical vapor deposition (CVD) diamond as secondary stage anvils materials. The ds-DAC designs (*18*, *19*) proved to be very efficient, with pressure generation of several megabars without sacrificing the first-stage diamond anvils, and showed that the yield strength of secondary-stage anvil material plays a decisive role in achieving ultrahigh pressures above 400 GPa (*13*, *15*, *18*, *19*).

Here, we report on the HPHT synthesis of transparent microballs of nanodiamond with unique microstructure and extraordinary mechanical and x-ray optical properties. Used as the secondary-stage anvils, the NCD balls allowed us to achieve ultrahigh static pressures beyond 1 TPa in a ds-DAC. We have also extended the capabilities of the ds-DAC due to the introduction of an internal gasket assembly, that is, a secondary pressure chamber inside the ds-DAC. This gasketed ds-DAC technique provides the capability to confine not only solid matter but also liquids and gases between the two NCD mianvils of the ds-DAC for further experiments at multimegabar ultrahigh static pressures.

[1]Material Physics and Technology at Extreme Conditions, Laboratory of Crystallography, University of Bayreuth, D-95440 Bayreuth, Germany. [2]Bayerisches Geoinstitut, University of Bayreuth, D-95440 Bayreuth, Germany. [3]Electron Microscopy for Materials Science (EMAT), University of Antwerp, Groenenborgerlaan 171, B-2020 Antwerp, Belgium. [4]European Synchrotron Radiation Facility, BP 220 F-38043 Grenoble Cedex, France. [5]Center for Advanced Radiation Sources, University of Chicago, Chicago, IL 60437, USA. [6]Institute for Photon Science and Synchrotron Radiation, Karlsruhe Institute of Technology, P.O. Box 3640, 76021 Karlsruhe, Germany. [7]ANKA Synchrotron Radiation Facility, Karlsruhe Institute of Technology, P.O. Box 3640, 76021 Karlsruhe, Germany. [8]Immanuel Kant Baltic Federal University, RU-236041 Kaliningrad, Russia.
*Corresponding author. Email: natalia.dubrovinskaia@uni-bayreuth.de
†These authors contributed equally to this work.
‡Present address: Center for Electrochemical Energy Storage, Skolkovo Institute of Science and Technology, 143026 Moscow, Russia.

RESULTS

NCD microball synthesis and selection

The NCD microballs with diameter of 10 to 20 μm were synthesized using glassy carbon as a precursor in multianvil apparatus at a pressure of 18 GPa and temperature of 2000°C in an MgO pressure-transmitting medium (*21*). Only optically transparent NCD balls (Fig. 1A) with a Raman spectrum characteristic for nanodiamond (Fig. 1B) were selected for the present study.

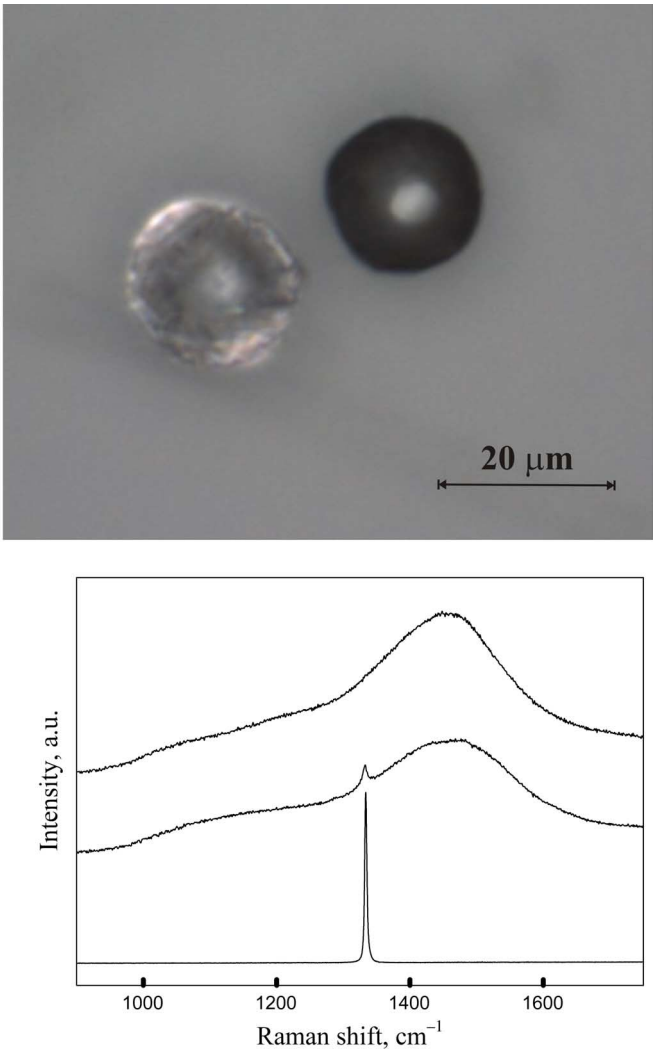

Fig. 1. Images of NCD balls and their Raman characteristics. (**A**) NCD balls as seen under an optical microscope: a transparent ball (left) and translucent one in the same field of view. (**B**) Raman spectra obtained from microballs of different crystallinity. Top curve corresponds to transparent NCD [synthesis conditions: *P* (pressure), 18 GPa; *T* (temperature), 2000°C; MgO pressure medium], whereas middle curve corresponds to translucent nanodiamond containing a small amount of polycrystalline component (18 GPa, 1850°C; MgO). For comparison, bottom curve presents a typical Raman spectrum of polycrystalline or single-crystal diamond. Only those microballs that showed a Raman spectrum characteristic for nanodiamond (without the diamond Raman peak A_{1g} at ~1331 cm^{-1}) were selected for the present study. a.u., arbitrary units.

Mechanical properties of the transparent NCD microballs

Following the methodology described earlier (*13*), we investigated the compressibility of the transparent NCD microballs and their strength under confining pressure using the DAC technique with in situ synchrotron x-ray diffraction. For this purpose, a ball is squeezed between two diamond anvils, as shown schematically in Fig. 2A. For all our experiments, we used piston-cylinder–type DACs with a large optical aperture produced at the Bayerisches Geoinstitut (BGI) (*22*, *23*) and diamonds with culet sizes of 120, 250, or 300 μm. A photograph of a real pressure chamber of a DAC taken under an optical microscope through the diamond "window" is shown in Fig. 2B. The diameter of the pressure chamber (that is, the size of the hole in the rhenium gasket) holding the ball is initially 125 μm. A high-magnification phase-contrast x-ray image of the NCD ball in this DAC (Fig. 2C) is obtained from high-resolution transmission x-ray microscopy (HRTXM) (*24*, *25*) using coherent high-energy synchrotron radiation.

The pressure profile across the microball and the pressure chamber is shown in Fig. 2D. The maximum pressure was obtained on top of the microball (P_{mb}), and the minimum pressure was recorded in the pressure chamber (P_{ch}). The P_{mb} was measured in different experiments using x-ray diffraction from a Re foil placed at the interface of the microball and the culet of the diamond anvil and/or by means of Raman spectroscopy, using the position of the high-frequency edge of the diamond Raman band [see study by Akahama and Kawamura (*26*) and references therein]. In each case, x-ray diffraction and Raman spectra were collected at the contact point "microball–Re–diamond anvil," which is easily identified as the black dot in the central part of Fig. 2C. In addition to the diamond scale, the ruby fluorescence scale was used to monitor P_{ch}; for this purpose, a ruby ball was placed into a pressure chamber (Fig. 2A). The microball shown in Fig. 2B remained intact after decompression to ambient conditions.

Figure 3 shows the unit cell volume of NCD as a function of pressure. At pressures above ~33 GPa, the NCD microball seems to become more compressible, but the observed effect is a consequence of bridging of the microball between the DAC's anvils and the development of deviatoric stresses (*13*). The experimental pressure-volume data (Fig. 3, dots) up to 33 GPa were fitted using the third-order Birch-Murnaghan equation of state (EOS) (Fig. 3, line) and gave the values of the bulk modulus K_{300} = 482(5) GPa, K' = 3.2(2), and V_0 = 3.393(3) cm^3/mol, which agree with those previously determined for aggregated diamond nanorods (*10*) and translucent NCD balls (*13*). Compared to the bulk moduli of single-crystal diamond and NPD (440 to 442 GPa) (*27*), the NCD bulk modulus appears to be larger.

The ability of the NCD balls to support significant stresses was already noticed in experiments with the translucent material. Their yield strength was evaluated to be 144 to 168 GPa (*13*) based on a comparison of the pressure in the chamber P_{ch} (in a pressure-transmitting medium) and the pressure (stress) P_{mb} over the NCD microball in contact with the diamond anvils (Fig. 2). Experiments with transparent NCD microballs bridged between the DAC anvils show that P_{mb} may reach 226(5) GPa (without any structural changes in NCD, it is detectable from the diffraction patterns), whereas P_{ch} is only 72(2) GPa. This gives a shear stress [$\tau = 1.5 \times (P_{mb} - P_{ch})$] of τ = 231(11) GPa and a yield strength ($Y = 2 \times \tau$) of Y = 462(22) GPa. Values of the yield strength of single-crystal diamonds reported so far are scattered: on the basis of the results of shock wave experiments, a maximum of 80 GPa was reported for the <110> direction at a confining pressure of approximately 55 GPa (*28*); DAC experiments gave a maximum of 130 to 140 GPa for the <100>

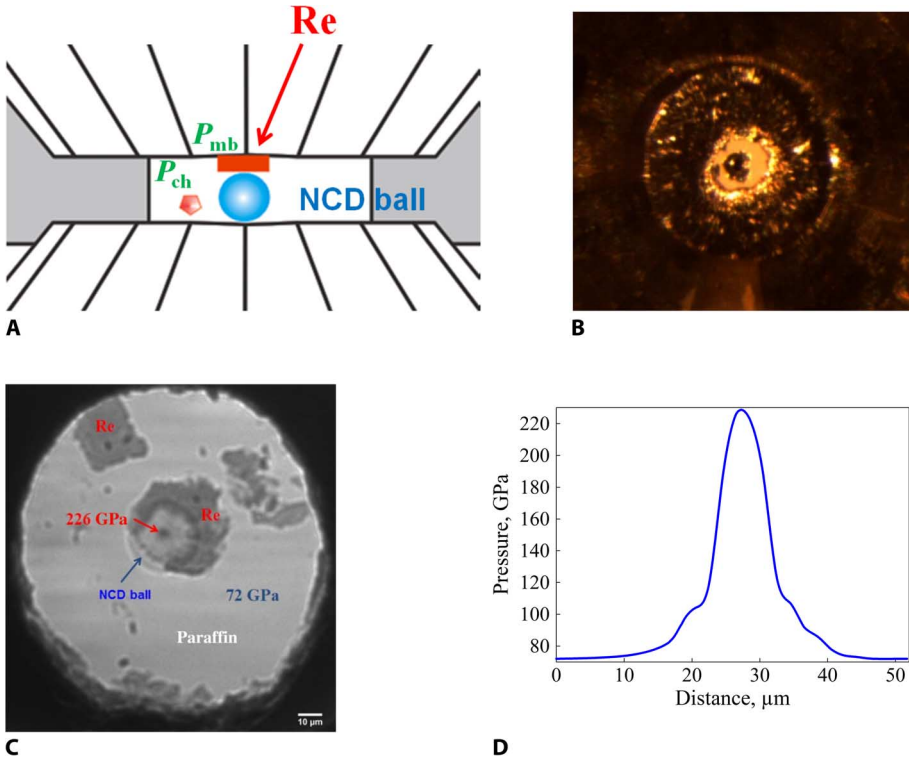

Fig. 2. The scheme of the experiment on the measurement of the yield strength of an NCD microball. (**A**) Schematic showing a pressure chamber with an NCD ball squeezed between two diamond anvils. The pressure exactly above the microball (P_{mb}) and the pressure inside of the pressure chamber (P_{ch}) were measured as described in the text [see also two separate studies by Dubrovinsky *et al.* (*5*, *13*) for details]. The pressure chamber was filled with paraffin used as a pressure-transmitting medium. (**B**) Image of a real pressure chamber of a DAC taken under an optical microscope through the diamond window. (**C**) High-magnification image of the NCD ball in this DAC. (**D**) Pressure profile across the pressure chamber (see text for details).

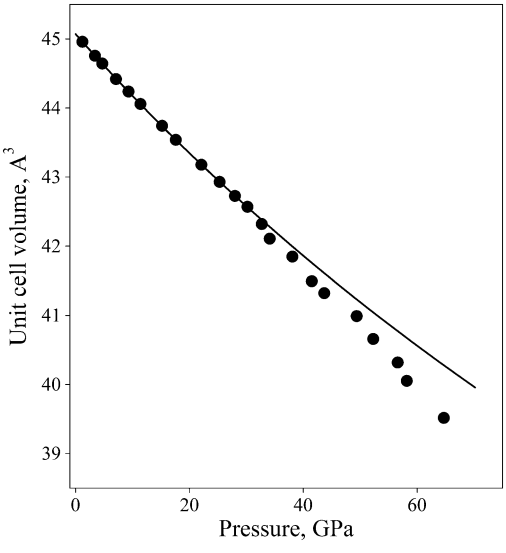

Fig. 3. The unit cell volume of NCD as a function of pressure. At pressures above ~33 GPa, the NCD microball seems to become more compressible, but the observed effect is a consequence of bridging of the microball between the DAC's anvils and the development of deviatoric stresses (*13*). Error bars are within the size of the dots.

direction at a load exceeding 200 GPa (*29*); for translucent NCD, up to 168 GPa (*13*) was reported under a confining pressure of 60 GPa, whereas theory predicts a maximum of 200 GPa (*30*) under compression in the <100> direction. Thus, the transparent isotropic NCD microballs that we synthesized from glassy carbon, at a confining pressure of 72 GPa, demonstrate an exceptional yield strength (at least three times higher than that of single-crystal diamonds) than ever reported or predicted for diamonds.

As described above, in our experiments, NCD microballs were bridged between the anvils, and the stress above 220 GPa that was achieved at their interface exceeded the yield point of single-crystal diamond, leading to a plastic deformation of the anvils. An inspection of the anvils using scanning electron microscopy after opening the DACs revealed round indents similar to those observed on materials after macroindentation tests using ball-shaped Brinell indenters (fig. S1). Diamond anvils with culets of different crystallographic orientations were then tested purposely (fig. S1). On the (100) face, we observed the first detectible sign of indentation at pressure above 105 GPa, whereas on the (111) face, it is observed at pressure above 120 GPa, in accordance with their relative hardness (*11*, *16*). On the NPD (*17*) anvil, an indent was observed at contact pressures above 150 GPa (fig. S1), which qualitatively confirms that NPD is harder than single-crystal diamond. In turn, the observed ability of the transparent NCD microballs to produce an indentation on the surface of the hardest known materials proves their

ultrahigh hardness. However, its quantification, that is, providing meaningful values of hardness, is not possible because a hardness scale for materials harder than diamond is yet to be developed.

Microstructure of transparent NCD balls

The microstructure of the NCD ball material was investigated using aberration-corrected transmission electron microscopy (TEM) and spatially resolved electron energy loss spectroscopy (EELS). The material consists of diamond nanograins with sizes ranging from 2 to 15 nm in diameter (Figs. 4, A and B, and 5A). High-resolution TEM (HRTEM) images of the diamond nanoparticles (Fig. 4, A and B) demonstrate that the grains have a crystalline diamond structure confirmed by electron diffraction (Fig. 5A). Most of the NCD nanoparticles have extremely small dimensions of 3 to 9 nm (Fig. 5A), implying that the grain boundaries become a very substantial part of the bulk material. The volume fraction of the grain boundaries may be estimated to be up to ~25%, if an average nanograin size of 5 nm is used for this evaluation, in correspondence with the histogram in Fig. 5A. The boundaries between the individual diamond grains (marked with black arrows in Fig. 4A) are not coherent, with a large fraction of the sp^2-bonded carbon that is concentrated within a thin (~0.5 nm) layer surrounding the diamond grains, as confirmed by EELS mapping (Fig. 4, C to E). We used the amorphous carbon reference, because this gave the best fit of the π^* peak at 285 eV, which is directly related to the presence of sp^2-hybridized carbon (and not to sp^3-hybridized carbon, which is related to the σ^* contribution around 292 eV). The disordered nature of the graphene-like

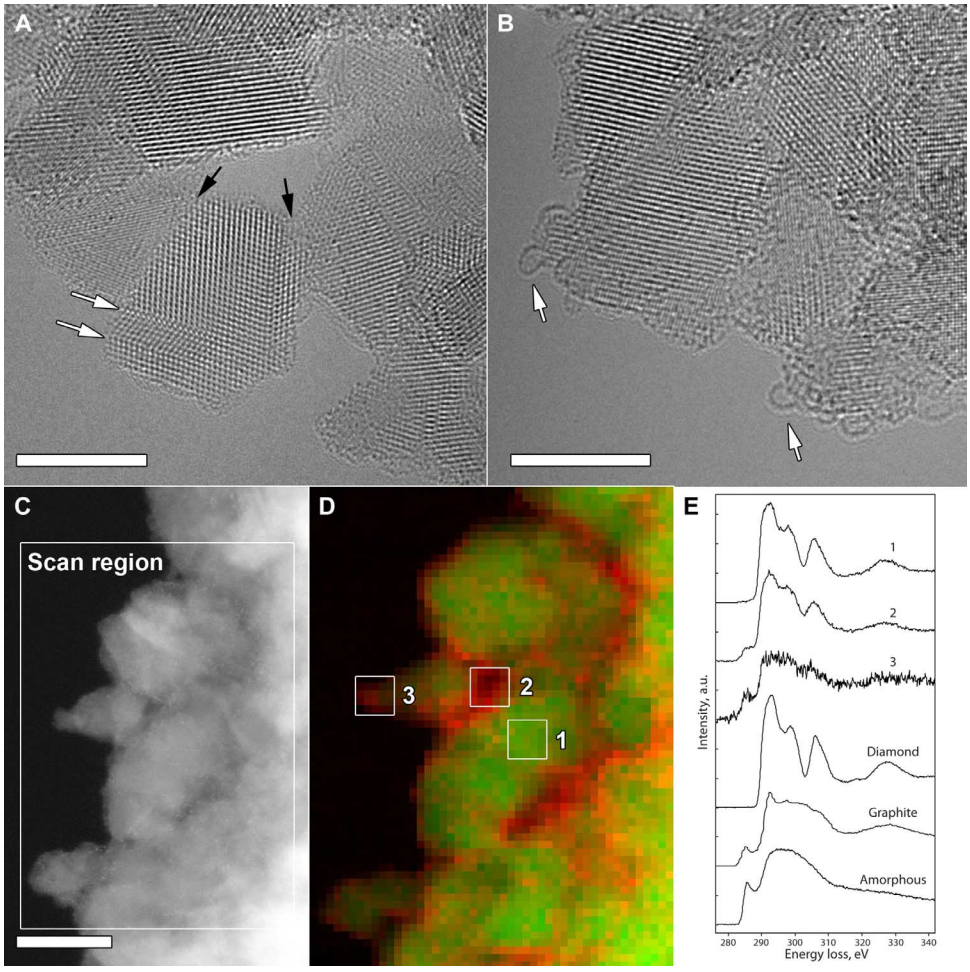

Fig. 4. The results of HRTEM and high-angle annular dark-field scanning TEM investigations. (**A** and **B**) Aberration-corrected HRTEM images of the diamond nanoparticles. Scale bars, 5 nm. (A) The boundaries between the individual diamond grains (marked with black arrows) are not coherent and often appear to be disordered. White arrows indicate the {111} twin planes. (B) Surface layer around the diamond nanoparticles forming fullerene-like reconstructions (marked with arrows). (**C**) High-angle annular dark-field scanning TEM (HAADF-STEM) image of a typical region of the diamond nanocrystals. Scale bar, 5 nm. This region was scanned using spatially resolved EELS, collecting the carbon-K edge. (**D**) Color map of the EELS signal depicting the sp^3-bonded carbon in green and the sp^2-bonded carbon in red. The color map was generated by fitting each pixel in the acquired EELS data set with a diamond and amorphous carbon spectral reference in a linear combination and plotting the diamond component strength in green and the amorphous carbon component strength in red. (**E**) EELS spectra measured from the areas indicated in (D), showing the fine structure of the C-K edge along with the standard spectra from diamond, graphite, and amorphous carbon. The spectrum from region 1 corresponds to diamond-like sp^3-bonded carbon, that from region 2 is a combination of the diamond and graphitic-like contributions, and that from region 3 is reminiscent of graphitic-like sp^2-bonded carbon.

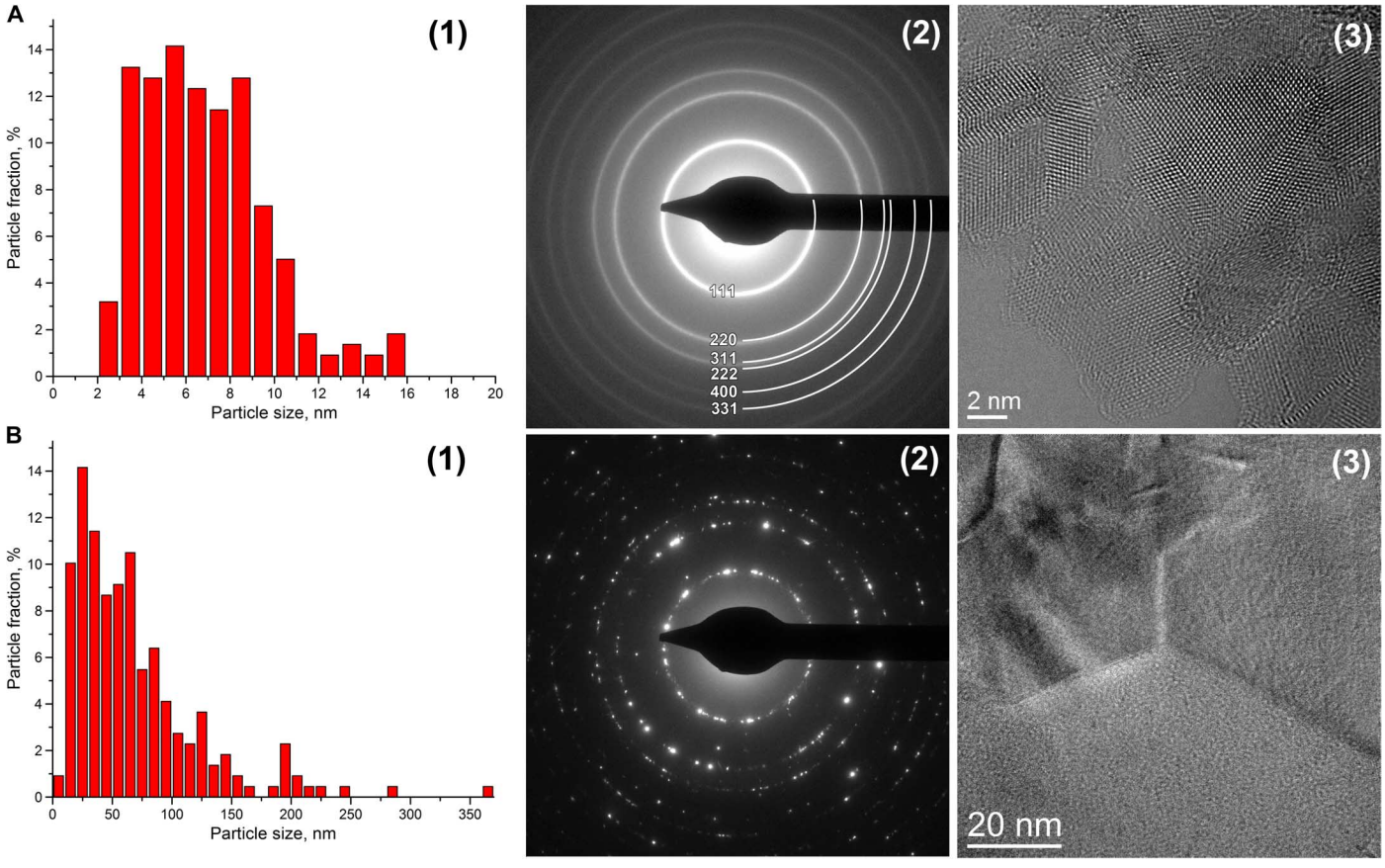

Fig. 5. Microstructure of NCD and NPD materials. (**A**) NCD. (**B**) NPD. Grain-size statistics (1), electron diffraction pattern (2), and grain imaging (3) give evidence to different microstructures of NCD and NPD. Most of the diamond nanograins in NCD have sizes in the range of 3 to 10 nm, whereas the diamond grains in NPD include submicrometer particles. The electron diffraction pattern of NCD shows continuous diffraction rings characteristic of nanocrystalline materials, whereas the pattern of NPD is spotty, as expected for materials containing quite coarse grains. The particle size was measured manually from dark-field TEM images on 218 and 219 particles for the NCD and NPD materials, respectively.

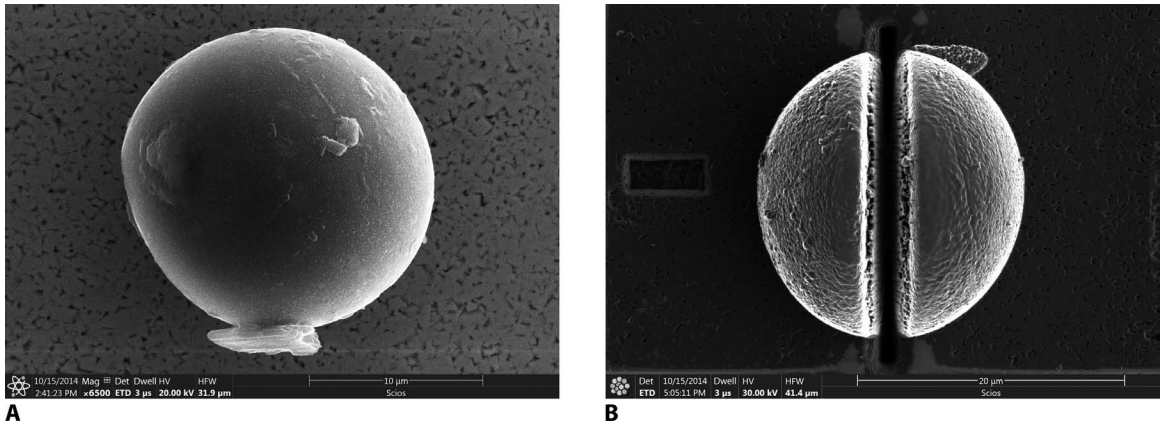

A B

Fig. 6. Images of an NCD ball before and after the FIB milling. (**A**) Secondary electron image of a ball before ion milling, as taken in the Scios DualBeam system (FEI Deutschland GmbH) at a voltage of 20 kV and a current of 0.8 nA. mag, magnification; Det, detector; ETD, Everhart Thornley detector; HV, high voltage; HFW, horizontal field width. (**B**) Gallium ion image of the same ball (taken at 30 kV and 30 pA) after milling at 30 kV and 5 nA.

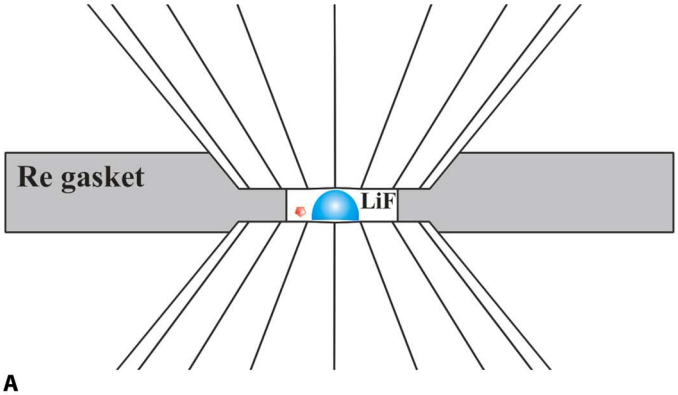

A

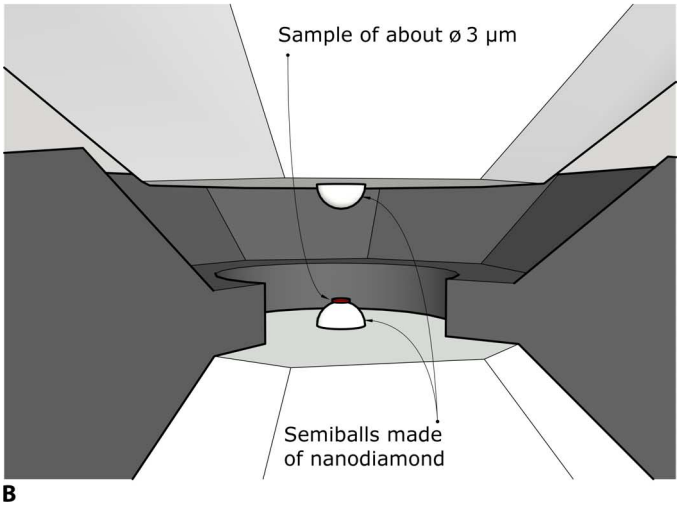

B

Fig. 7. Schematic drawings of the setup for ultrahigh static pressure generation. (**A**) Testing of the performance of a single semiball forced against the diamond anvil in a LiF pressure medium in a conventional DAC. (**B**) ds-DAC assembly (not to scale) for experiments at ultrahigh pressures (above 1 TPa). Two transparent NCD semiballs were used as secondary anvils in a conventional DAC. Diameter of the NCD semiballs is ~20 μm, and the initial size of the sample is about 3 μm in diameter and about 1 μm in thickness.

material at the surface of the nanodiamond grains causes this broadening (Fig. 4E, curve 3) as compared to pure graphite (Fig. 4E). We have not quantified the sp^2 to sp^3 ratio because the data were not acquired under the so-called magic angle conditions needed for quantitative interpretation of EELS signals from anisotropic materials, like graphite, meaning the area under the π^* peak is dependent on the amount of sp^2 carbon in the probed region and orientation of the specimen. The color map is displayed as a qualitative map showng the presence of sp^2 carbon at the surface of the nanodiamond grains.

It is worth mentioning that the thickness of the grain boundaries in the NCD is comparable with the thickness of a single layer of graphene, which is normally approximately 0.35 nm. The transparency of the single layer of graphene is approximately 96.4% (for the two layers, it is still 92.7%) (see, for example, www.tedpella.com/Support_Films_html/Graphene-TEM-Support-Film.htm; PELCO Graphene TEM Support Films), which can explain why the NCD balls may be transparent despite a considerable fraction of the sp^2-bonded carbon. The "graphene"-like layer at the surface of the grains locally forms fullerene-like reconstructions (Fig. 4B). These observations are in line with the results of ab initio calculations of the grain boundary and the surface structures of diamond nanocrystals (*31*, *32*).

A comparison of the microstructure of NCD with that of NPD allows us to conclude that these two diamond materials are considerably different. Figure 5 shows the grain size statistics, electron diffraction patterns, and grain boundary images for NCD (Fig. 5A) and NPD (Fig. 5B). Most of the diamond nanograins in NCD have sizes ranging from 3 to 10 nm, whereas the diamond grains in NPD are substantially larger and include submicrometer particles. The electron diffraction pattern of NCD shows broadened continuous lines characteristic for nanocrystalline materials, whereas the pattern of NPD is spotty, as expected for materials containing quite coarse grains. The grain boundaries in NCD are incoherent and very narrow, whereas those in NPD are straight: they resemble the planar directions in the diamond structure. A unique combination of exceptional strength of the graphene-like grain boundary and high hardness of diamond nanoparticles results in superior mechanical properties of NCD.

Ultrahigh static pressure generation

To use the unique mechanical and optical properties of NCD, which originate in the microstructure of the material, we tested the performance of the NCD semiballs as secondary anvils for the generation of ultrahigh pressures. Semiballs of NCD were prepared by milling NCD balls using focused ion beam (FIB) technique (Fig. 6) and cleaned in boiling aqua regia for 30 min. One of the semiballs was loaded in a LiF pressure medium into a conventional DAC (Fig. 7A) equipped with beveled CVD diamond anvils (120-μm culets). The tip of the semiball was pressed against the opposite anvil until a pressure of ca. 100 GPa was measured in the sample chamber using the ruby fluorescence scale (Fig. 7A). The maximum pressure under the tip, recorded using the Raman shift of the high-frequency edge of the diamond mode (fig. S2) (*26*), reached about 460 GPa, following the extrapolation of the diamond calibration in the study by Akahama and Kawamura (*26*).

The NCD remains optically transparent up to the highest pressure achieved in this experiment. Moreover, infrared (IR) spectroscopy confirms that the NCD semiball does not cause any additional spectral features compared to diamond anvils (fig. S3). It merely reduces the overall intensity, most probably because of its curved shape. This finding makes NCD a material of choice for ultrahigh-pressure IR spectroscopy studies in a wide spectral range.

In a second run, two transparent semiballs of ~20 μm in diameter were used as secondary anvils in a ds-DAC (Fig. 7B) (*13*). A pair of 16-sided (100)-oriented beveled diamonds with culets of 120 μm in diameter was used as primary anvils, and a rhenium gasket was preindented to a thickness of ~27 μm to ensure that the first contact between the secondary anvils happens only when the chamber pressure is above ~25 GPa. The sample was a gold foil [with 99.9995% purity and lattice parameter of 4.07865(9) Å at ambient condition] with an initial thickness of 1 μm and a diameter of less than 3 μm (Fig. 7B), placed at the tip of one of the semiballs using the micromanipulator (Micro Support Co. Ltd.). Paraffin wax was used as the pressure-transmitting medium in the sample chamber. The cell was pressurized over 70 GPa (as measured on the Raman peak from the culet of primary diamond anvil) at BGI and transferred to the 13 IDD [GeoSoilEnviroCARS (GSECARS)] beamline at the Advanced Photon Source (APS; United States) where high-resolution in situ x-ray diffraction experiments were performed. The

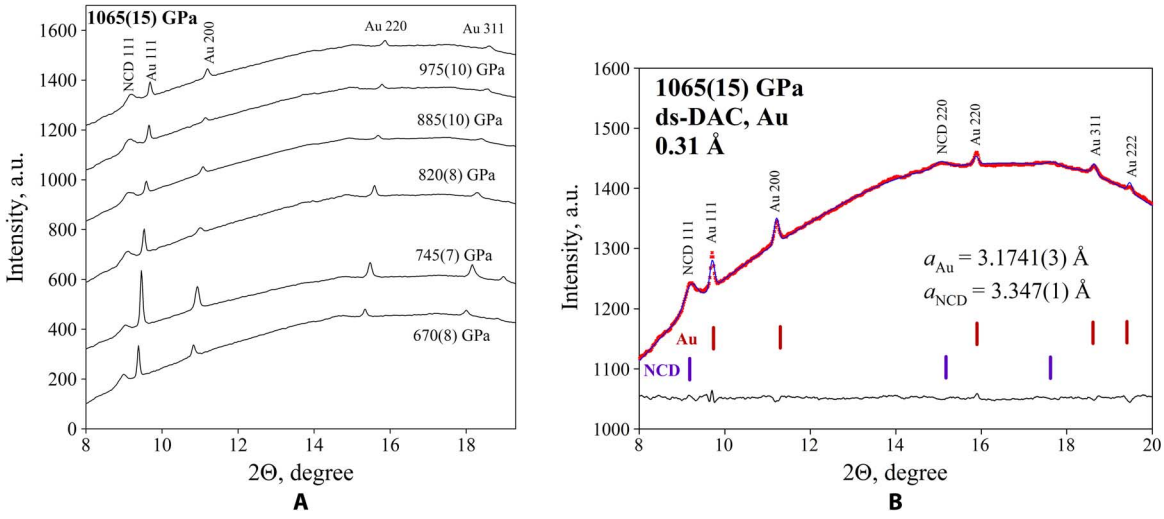

Fig. 8. The synchrotron powder x-ray diffraction data of gold subjected to pressures above 1 TPa in a ds-DAC. (**A**) Sequence of the diffraction patterns obtained at ultrahigh pressures above 670 GPa. (**B**) GSAS plot for the diffraction data collected at a pressure of 1065(15) GPa for 120 s with an x-ray wavelength of λ = 0.31 Å. Red dots indicate the experimental points; blue curve, the simulated diffraction pattern; and dark line, the residual difference. A powder of Au was compressed in a ds-DAC using paraffin wax as a pressure-transmitting medium. The lattice parameter of gold is *a* = 3.1741(3) Å, and that of NCD is *a* = 3.347(1) Å. Pressure was determined according to the gold EOS (*5*, *33*).

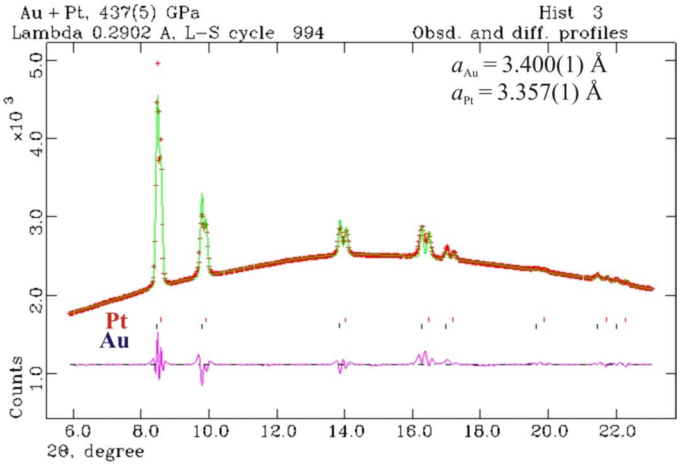

Fig. 9. Diffraction pattern of a mixture of gold [*a* = 3.400(1) Å] and platinum [*a* = 3.357(1) Å] compressed in a ds-DAC equipped with Bohler-Almax first-stage anvils. Experimental data are shown by red crosses; continuous green curve is due to simulation with the full-profile (GSAS) software. The pressures are 417(5) GPa, according to the platinum EOS, and 432(5) GPa, according to the EOS of gold [calculated using http://kantor.50webs.com/diffraction.htm; see also study by Fei *et al.* (*35*) and Dubrovinsky *et al.* (*5*)]. This small difference in pressures determined from the EOS of two metals with different mechanical and elastic properties suggests that possible effects of stresses are insignificant for Au (and Pt) at a multimegabar pressure range. Moreover, x-ray data were also collected in geometry, when the optical axis of a DAC is under the angle of 35° to the incident x-ray beam. This is possible due to a large (80°) opening of the DAC. In this geometry, we obtained the same (within uncertainties) positions of diffraction lines and the lattice parameters for both Pt and Au, compared to those in parallel geometry, thus confirming a negligible effect of stress. Obsd. and diff., observed and difference profiles.

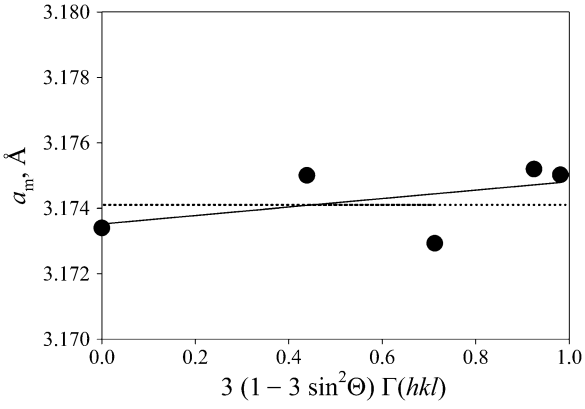

Fig. 10. The Γ plot for Au at 1065(15) GPa. Θ is the diffraction angle, and a_m is the unit cell parameters calculated from the individual *d* spacings ($d_{observed}$) from table S1 for the *hkl* 200, 311, 220, 222, and 111 (dots from left to right). The line is a linear fit through experimental data points (dots); the dashed line shows the value of the lattice parameter obtained by the full-profile (GSAS) fitting. On the basis of these data and following the methodology described in the studies by Dorfman *et al.* (*34*) and Takemura and Dewaele (*36*), the maximal unixial stress component was evaluated to be less than 20 GPa, in good agreement with extrapolations of data of earlier measurements (*34*, *37*).

diffraction pattern (Fig. 8) consists of several reflections of gold and the very broad (111) reflection of the nanodiamond (other diamond reflections are almost invisible due to very small sizes of the NCD crystallites that resulted in significant broadening of reflections). The pressure in the primary chamber was increased in several steps (Fig. 8 and fig. S4) up to about 125 GPa. At pressures above ~90 GPa in the chamber (when the pressure between the tips of the NCD secondary anvils

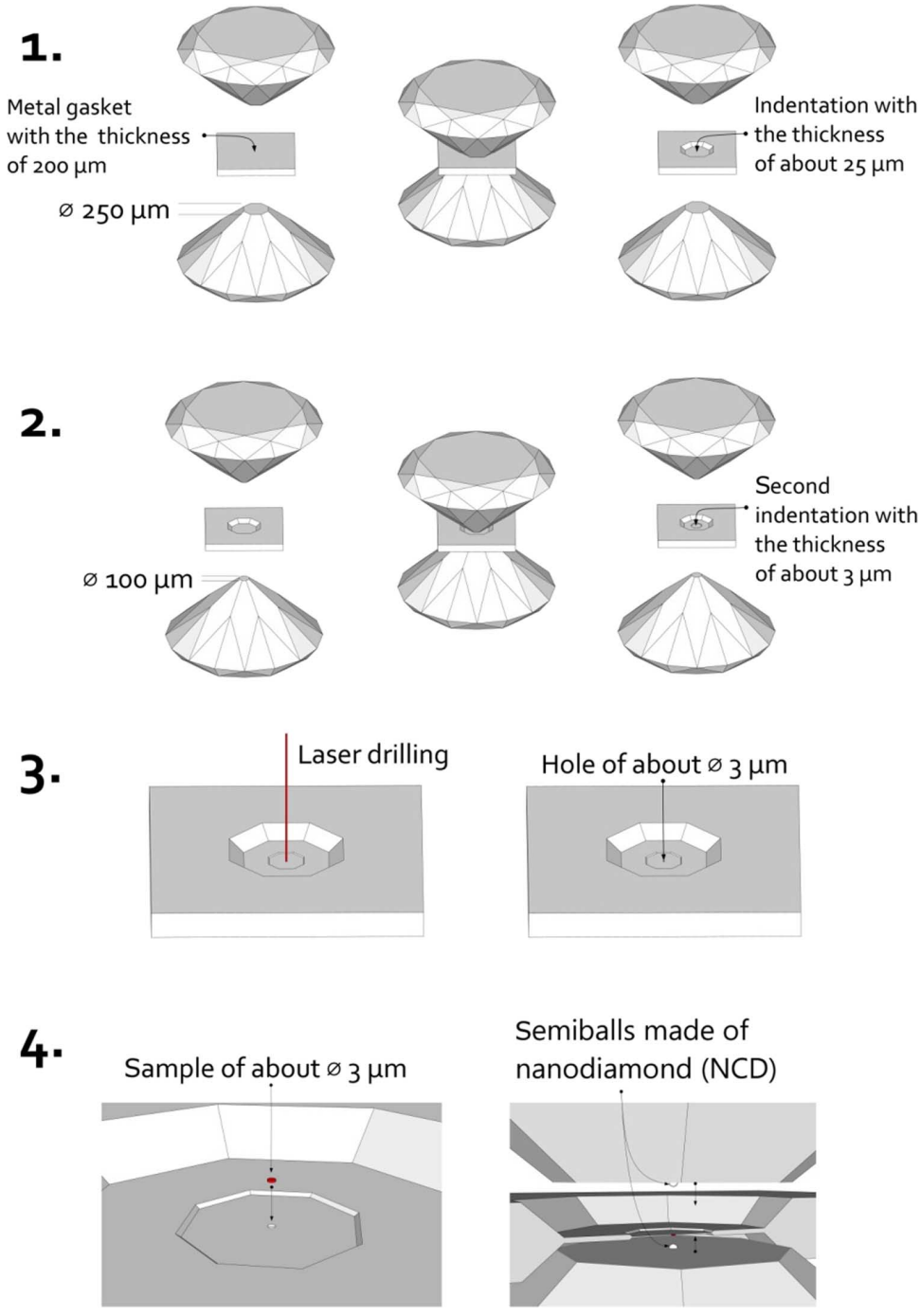

Fig. 11. Scheme of the gasket preparation for ds-DACs. (1) A rhenium foil with an initial thickness of ~200 μm is indented to ~25 μm using a conventional DAC with diamond anvils having culets of 250 μm. (2) In the middle part of the initial indentation, an additional indentation with a final thickness of ~3 μm is made using 100-μm culet diamonds. (3) Using a pulsed laser, a hole with a diameter of ~3 to 4 μm is drilled at the center of the secondary indentation. (4) A sample (Au or Pt in our experiments) is loaded using the micromanipulator into the center of the secondary pressure chamber. NCD semiballs (secondary anvils) are attached to the gasket using traces of wax, and the whole assembly is mounted on the primary anvils (with either flat 250-μm or beveled 120-μm culets in our experiments). Empty space in the secondary chamber in our experiments was filled by wax or by Ar (loaded at 1.3 kbar).

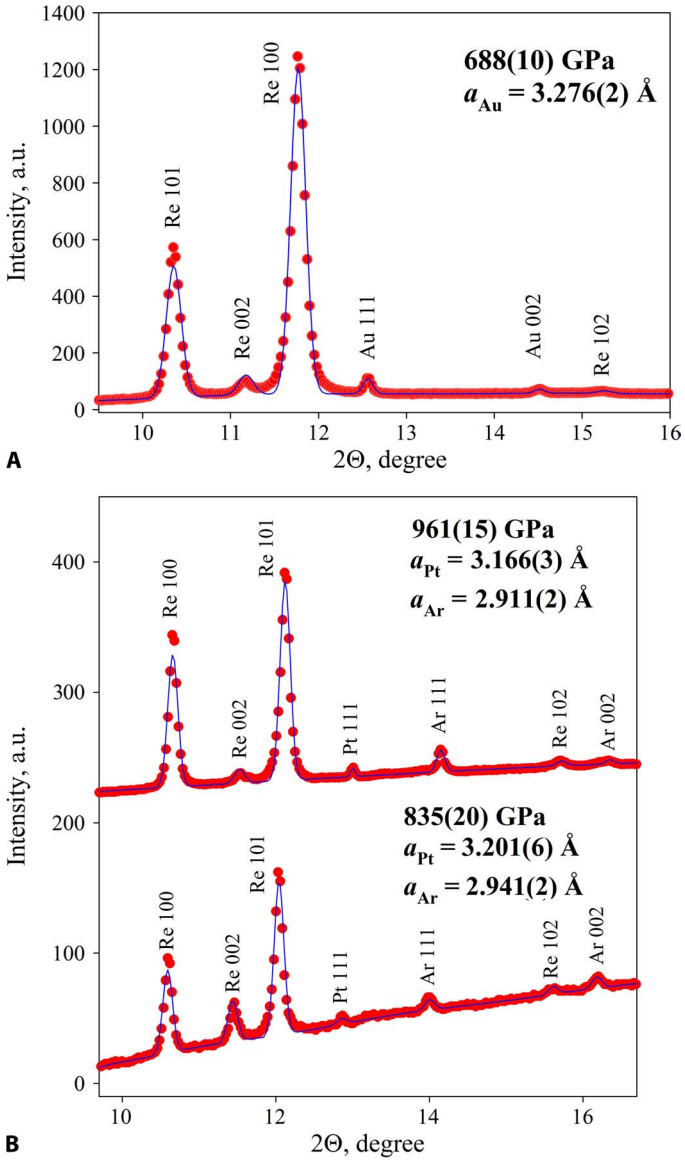

Fig. 12. Examples of the diffraction patterns collected in gasketed ds-DACs. (**A**) Mixture of Au and paraffin wax at 688(10) GPa [pressure is given on the basis of the lattice parameter of gold and the EOS from Yokoo *et al.* (*33*)]. (**B**) Platinum compressed in argon. Pressure is given on the basis of the Pt EOS from Yokoo *et al.* (*33*). Rhenium reflections are due to gasket material compressed between primary anvils to about 60 GPa (A) and 120 and 135 GPa (B); although the full width at half-maximum (FWHM) of the x-ray beam is about 2 μm, the tails of the beam are intense enough to result in strong scattering by a large amount of rhenium surrounding the samples. Diffraction patterns were collected using x-ray with wavelength of ~0.41 Å and processed with the GSAS Software (red dots indicate experimental points, whereas blue lines indicate calculated values).

exceeds 800 GPa), the NCD (111) reflection became asymmetric with a clear shoulder at lower *d* spacing, which may be due to the high stress in the secondary anvils (although we cannot fully exclude structural changes in the NCD material at such extreme conditions). Whereas the intensity of the gold reflections decreases with increasing pressure, gold is perfectly visible in the diffraction patterns even at the highest pressure achieved, and the quality of the data is sufficient for a full-profile refinement (Fig. 8). The smallest lattice parameter of gold measured in our experiment is 3.1741(3) Å (Figs. 8 to 10, fig. S4, and table S1), which corresponds to 1065(15) GPa, according to the Au EOS of Yokoo *et al.* (*5*, *33*). Use of other available Au EOS gives almost the same or even higher pressure values: 1090(15) GPa (*34*) or 1125(15) GPa (*35*). According to very recent investigations, the stress field generated by the second-stage anvils is very similar to one of the conventional DAC experiments (*5*, *19*). The uniaxial stress component evaluated on the compression of gold in ds-DAC (*19*) increases linearly with pressure and reaches ~2.5 GPa at ~225 GPa and, thus, could be expected to be around 10 GPa at 1 TPa. Following the methodology described in the studies by Dorfman *et al.* (*34*) and Takemura and Dewaele (*36*), the maximal uniaxial stress component on gold in our experiments (Fig. 10 and table S1) is estimated to be less than 20 GPa at maximum pressure reached in good agreement with extrapolations of data of earlier measurements (*34*, *37*), and is therefore relatively insignificant. Thus, because of the enormous yield strength of the NCD microballs proven in this study, a pressure above 1 TPa was reached on the gold sample.

Internal gasket in the ds-DAC

So far, ds-DACs were used without gaskets, and samples were compressed directly between secondary anvils (*5*, *18*, *19*). This limited the application of the technique only to solid materials. In combination with our novel NCD material, able to sustain much larger stresses compared to strong materials known before, we developed the technique of secondary gasket preparation (Fig. 11) and introduced an internal gasket for ds-DACs. In one experiment, a rhenium gasket was indented in two steps using 250- and 100-μm diameter diamonds down to a thickness of 3 μm. A pressure chamber of ~3 μm was drilled, loaded with a mixture of gold and paraffin wax, and compressed to 688(10) GPa (Fig. 12). Upon compression, the diameter of the pressure chamber increased up to about 5 μm, and gold appeared to occupy only a portion of the pressure chamber. As a result, we could observe light (fig. S5) passing through the pressure medium (paraffin wax) compressed to almost 700 GPa, which confirms that NCD remains optically transparent even at such high pressures.

Gasketed ds-DACs extend the capabilities of investigation of material at ultrahigh pressure, and it is now possible to even gas-load sample in between the semispheres. For example, platinum was loaded with Ar at 1.3 kbar and pressurized using beveled first-stage anvils first to 120 GPa and then to 135 GPa (Fig. 12). Diffraction peaks of both Pt and Ar are identifiable. Pressure achieved between the secondary anvils is not easy to characterize precisely because of the absence of the experimental EOS of Pt above ~600 GPa (*33*) and Ar (*38*) above ~100 GPa (Fig. 12). Still, available EOS data suggest that materials have been compressed up to about 800 to 970 GPa. Using different EOS, provided in table S1 of the study by Yokoo *et al.* (*33*), and about two- to eight-time extrapolations for Pt, we get pressures 717 to 840 GPa for a = 3.201(6) Å and 812 to 970 GPa for a = 3.166(6) Å. With about 10-time extrapolation for Ar [see study by Marquardt *et al.* (*38*) and references therein], pressure estimates range from 491 to 1075 GPa for a = 2.941(2) Å and from 540 to 1185 GPa for a = 2.911(2) Å.

NCD balls as x-ray divergent lenses

The NCD balls not only have unique mechanical properties (complex elasticity, ultrahigh hardness, and yield strength) but also

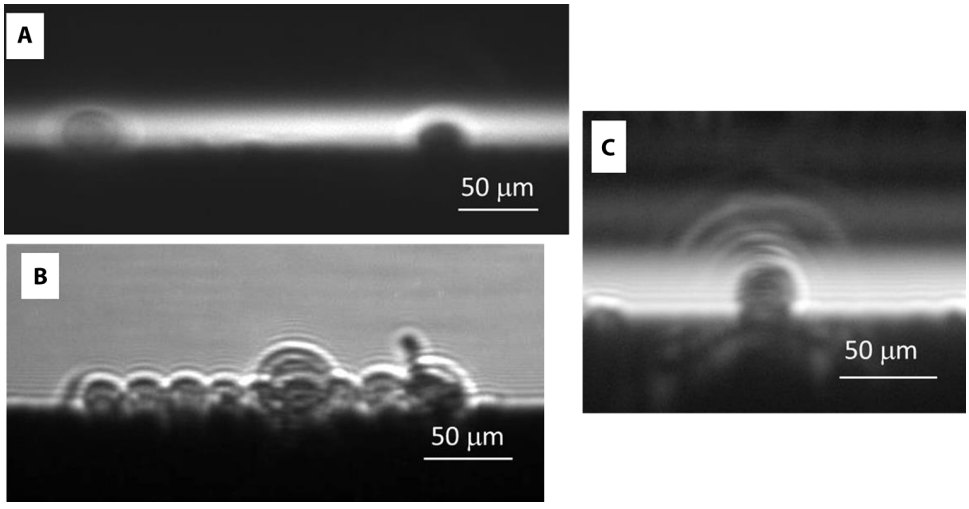

Fig. 13. X-ray images of the nanodiamond balls. (**A**) A single ball (left) and nine balls aligned in the direction of the x-rays (right), along the direction of view. The single ball is practically transparent, whereas the nine aligned balls look black because their set negatively focuses the light (it is seen that the nine balls are well aligned along the optical axis). (**B**) X-ray image of the same balls taken in the direction perpendicular to that of the alignment of the nine balls; the single ball (biggest one) is seen at about the center of the image. Primary slits were closed down to 50 μm; therefore, a nice interference pattern is seen around the balls. (**C**) X-ray image showing the divergent beam passing the negative lens. This negative diamond lens of nine aligned balls was tested on ID06 beamline at ESRF where a 10 μrad divergent 12-keV x-ray undulator beam was expanded to 100 μrad, giving an angular divergence value of 2×10^{-4}.

are structurally isotropic, homogeneous, and made of a low-Z material, making them excellent candidates in the field of x-ray optical applications. High-quality diamond spheres are a classical example of x-ray divergent (negative) lenses. We performed a test of the diverging properties of a lens consisting of a stack of nine NCD balls (Fig. 13) at the microoptics test bench at the ID06 beamline of the European Synchrotron Radiation Facility (ESRF). The beam was produced by an in-vacuum undulator, and the desired 12-keV x-ray energy was selected by a cryogenically cooled Si (111) double-crystal monochromator. The lens was aligned along the x-ray beam by means of phase-contrast imaging with a high-resolution CCD (charge-coupled device) camera located at a distance of 40 cm from the lens. To perform the test of the diverging properties of the lens, we closed the vertical slits in front of the lens down to 25 μm to block the direct beam. The divergent x-ray beam was depicted with the CCD camera showing few arcs spread over the distance more than 50 μm. From this, the angular divergence as 2×10^{-4} can be estimated. Thus, we have proven that such a negative nanodiamond lens can cause parallel rays of light passing through it to diverge or spread out, which might be of great interest for the development of x-ray microcopy techniques (*24*, *25*). In view of the global trend toward the development of fourth-generation x-ray sources like x-ray free electron lasers and ultimate storage rings, the need for the beam expansion has become extremely important.

DISCUSSION

So far, "materials at static terapascal pressures" have been investigated only theoretically. Here, we synthesized and fully characterized a unique material with a capability of being used to generate static pressures above 1 TPa, as proven in synchrotron x-ray diffraction experiments. This makes a breakthrough in the high-pressure technology and high-pressure physics, chemistry, and materials research opportunities. Exploiting mechanical properties of the unique NCD material and a ds-DAC design (with a nongasketed or gasketed secondary pressure chamber) opens a way to experimentally investigate up to ultrahigh pressure physical and chemical evolution of not only solids but also materials that are liquid and gaseous at ambient conditions. This provides totally novel prospects for both new materials discoveries and verification of theories.

The considerable fraction of the noncrystalline material in the grain boundaries allows us to consider the NCD material as a nanocomposite. If so, the compressibility of NCD measured using x-ray diffraction relates only to the "diamond fraction" of the material, rather than to the bulk compressibility of the composite that has to be different. Bulk nanostructured materials consisting of crystalline component(s) and structurally different/disordered interfaces often demonstrate bulk elasticity that is dissimilar from that inferred from the behavior of the crystallites.

We would like to note that the relationship between the yield strength and the performance of a material as anvil is not so simple—single-crystal diamonds with the reported yield strength of a maximum of 140 GPa allow generating pressures in excess of 400 GPa. Untangling the structure-property relationship in the very specific NCD material is thus another important aspect of the present study. NCD consists of isometric nanometer-sized (3 to 9 nm) diamond grains linked together by a monolayer of graphene-like carbon that gives it an unusual and complex elasticity of a composite material, as described previously. Additional strengthening effect in our experiments originates from the "confining pressure" of the pressure medium in the primary chamber of a DAC. The yield strength value of ~460 GPa is the lower estimate for our NCD microballs; we could not evaluate the upper limit because the single-crystal diamond anvils deformed and yielded.

MATERIALS AND METHODS

Synthesis of optically transparent NCD balls was realized by direct conversion of commercially available glassy carbon balls to diamond in multianvil apparatus at high pressures and high temperatures. The HPHT synthesis technique has been described in detail elsewhere (*21*).

In situ x-ray diffraction high-pressure experiments were conducted at BGI (Germany), at ID09 ESRF (France), and at GSECARS (Sector 13) at APS (United States). Sources of possible contaminations of the studied samples were carefully analyzed; impurities, which could affect the diffraction patterns, were never detected. At BGI, we obtained powder x-ray diffraction data with a system consisting of a Rigaku FR-D high-brilliance generator (90 kW) and APEX CCD area detector. The Mo$K\alpha$ radiation (tube voltage, 60 kV; tube current, 55 mA; cathode gun, 0.1 × 0.1 mm) was focused with Max-Flux x-ray optics and further collimated down to 30-μm FWHM beam size. At the ID09 at ESRF, the data were collected with the MAR555 detector using the x-ray beam of ~0.41 Å in wavelength and beam size down to 5 × 5 μm^2. At 13 IDD station (GSECARS), experiments were performed using a Mar165 CCD area detector and a tightly focused beam (~3 × 4 μm^2) of 0.31 Å. The collected images were integrated using the FIT2D, Dioptas, and GADDS programs to obtain a conventional diffraction pattern. Data analysis was conducted using the GSAS (general structure analysis system) package (*39*, *40*).

HRTXM using coherent high-energy synchrotron radiation was performed at the micro-optics test bench at the ID06 beamline of the ESRF. The x-ray energy of 11.832 keV (~12 keV) was selected by a silicon double-crystal monochromator with $\Delta\lambda/\lambda$ ~10^{-4}. HRTXM was realized by using a condenser, an objective lens, and a CCD detector. The condenser consists of compound refractive lenses and four Be parabolic lenses with 200-μm radius of parabola apex, and provides a coherent illumination on the sample. It was placed at a distance of 38.7 m from the undulator source. The sample was placed on the translation/rotation stage with the translation direction along the beam axis. The objective lens is an assembly of 27 individual Be parabolic lenses with 50-μm radius of parabola apex. It was located 56 m from the source. High-resolution Sensicam CCD detector with a resolution of 1.3 μm (pixel size, 0.645 μm), used to record the images, was placed 4.798 m from the objective lens. The objective lens image distance (sample–to–objective lens distance) was 0.414 m. Thus, the magnification factor on the order of 11 and the final resolution of ~100 nm, limited by the pixel size, were achieved.

The TEM specimen was prepared by crushing 10 NCD balls between tungsten carbide anvils, dispersing the material in ethanol, and depositing it onto a holey carbon grid. HRTEM images, HAADF-STEM images, and EELS spectra in STEM mode were acquired on an aberration-corrected Titan-"cubed" microscope, operated at 120 kV, and equipped with a GIF Quantum spectrometer. EELS data were acquired using a convergence semiangle of 22 mrad and an acceptance inner semiangle of 36 mrad (*41*).

FIB milling of NCD balls was realized using FEI Scios DualBeam. The visualization and the eucentric height positioning of the NCD balls were made using secondary and backscattered electron at 0.8 nA and 20 kV generated by the scanning electron microscope column. A gallium beam of 5 nA at 30 kV was then used to mill the NCD balls over their entire diameter. To enhance the milling process, a selective carbon gas injection system was used. Finally, the surface was cleaned using Ga beam of 1 nA at 30 kV.

IR spectroscopy measurements were carried out on the IR2 beamline of the ANKA Synchrotron Facility, Karlsruhe, Germany. Spectra were acquired using a Fourier transform IR IFS 66v/S spectrometer coupled to an IRscope II microscope (Bruker Optics). The spectrometer was equipped with a KBr beamsplitter; the spectral resolution was set to 4 cm^{-1}, and 512 scans were accumulated for each spectrum at a scanner velocity of 80 kHz. Measurements were performed in normal incidence reflectance as well as in transmitted light mode using Schwarzschild objectives (15×; numerical aperture, 0.4) and a liquid nitrogen–cooled midband mercury cadmium telluride detector. The high brilliance of the synchrotron IR beam allowed restriction of the sample area sensed by the detector with an aperture of 20 μm. To eliminate the influence of the decay of the synchrotron electron beam current, a background spectrum was recorded from the gasket in reflectance and through the diamond anvils beside the NCD semisphere in transmission geometry before measurement of every sample. The sample environment of the IR microscope was closed with a N_2-purged enclosure box, maintaining an air humidity below 2%. For data acquisition and analysis, OPUS Software (Bruker Optics) was used.

SUPPLEMENTARY MATERIALS

Supplementary material for this article is available at http://advances.sciencemag.org/cgi/content/full/2/7/e1600341/DC1

fig. S1. Images demonstrating comparative hardness of NCD, single-crystal diamond, and NPD.
fig. S2. Raman spectra collected from the diamond anvil over the tip of a semiball and at its edge.
fig. S3. Reflectance IR spectra collected through and beside an NCD semiball compressed in a LiF medium at the IR2 beamline at ANKA Synchrotron.
fig. S4. Variations of the lattice parameters of gold (red circles) and NCD of secondary anvils (blue squares) as functions of the pressure in the chamber.
fig. S5. Optical photograph of the sample (Au and paraffin wax) compressed in a gasketed ds-DAC at 688(10) GPa, as seen through the diamonds and NCD secondary anvils.
table S1. Observed and calculated *d* spacing of Au at 1065(15) GPa.

REFERENCES AND NOTES

1. P. Dalladay-Simpson, R. T. Howie, E. Gregoryanz, Evidence for a new phase of dense hydrogen above 325 gigapascals. *Nature* **529**, 63–67 (2016).
2. A. P. Drozdov, M. I. Eremets, I. A. Troyan, V. Ksenofontov, S. I. Shylin, Conventional superconductivity at 203 kelvin at high pressures in the sulfur hydride system. *Nature* **525**, 73–76 (2015).
3. E. Kim, M. H. W. Chan, Probable observation of a supersolid helium phase. *Nature* **427**, 225–227 (2004).
4. I. G. Austin, N. F. Mott, Metallic and nonmetallic behavior in transition metal oxides. *Science* **168**, 71–77 (1970).
5. L. Dubrovinsky, N. Dubrovinskaia, E. Bykova, M. Bykov, V. Prakapenka, C. Prescher, K. Glazyrin, H.-P. Liermann, M. Hanfland, M. Ekholm, Q. Feng, L. V. Pourovskii, M. I. Katsnelson, J. M. Wills, I. A. Abrikosov, The most incompressible metal osmium at static pressures above 750 gigapascals. *Nature* **525**, 226–229 (2015).
6. M. Millot, N. Dubrovinskaia, A. Černok, S. Blaha, L. Dubrovinsky, D. G. Braun, P. M. Celliers, G. W. Collins, J. H. Eggert, R. Jeanloz, Shock compression of stishovite and melting of silica at planetary interior conditions. *Science* **347**, 418–420 (2015).
7. S. Yip, Nanocrystals: The strongest size. *Nature* **391**, 532–533 (1998).
8. T. Irifune, A. Kurio, S. Sakamoto, T. Inoue, H. Sumiya, Materials: Ultrahard polycrystalline diamond from graphite. *Nature* **421**, 599–600 (2003).
9. N. Dubrovinskaia, L. Dubrovinsky, F. Langenhorst, S. Jacobsen, C. Liebske, Nanocrystalline diamond synthesized from C_{60}. *Diam. Relat. Mater.* **14**, 16–22 (2005).
10. N. Dubrovinskaia, L. Dubrovinsky, W. Crichton, F. Langenhorst, A. Richter, Aggregated diamond nanorods, the densest and least compressible form of carbon. *Appl. Phys. Lett.* **87**, 083106 (2005).
11. H. Sumiya, T. Irifune, Hardness and deformation microstructures of nano-polycrystalline diamonds synthesized from various carbons under high pressure and high temperature. *J. Mater. Res.* **22**, 2345–2351 (2007).
12. C. Le Guillou, F. Brunet, T. Irifune, H. Ohfuji, J.-N. Rouzaud, Nanodiamond nucleation below 2273K at 15GPa from carbons with different structural organizations. *Carbon* **45**, 636–648 (2007).

13. L. Dubrovinsky, N. Dubrovinskaia, V. B. Prakapenka, A. M. Abakumov, Implementation of micro-ball nanodiamond anvils for high-pressure studies above 6 Mbar. *Nat. Commun.* **3**, 1163 (2012).
14. H. Sumiya, T. Irifune, Indentation hardness of nano-polycrystalline diamond prepared from graphite by direct conversion. *Diam. Relat. Mater.* **13**, 1771–1776 (2004).
15. N. Dubrovinskaia, S. Dub, L. Dubrovinsky, Superior wear resistance of aggregated diamond nanorods. *Nano Lett.* **6**, 824–826 (2006).
16. H. Sumiya, K. Harano, T. Irifune, Ultrahard diamond indenter prepared from nanopolycrystalline diamond. *Rev. Sci. Instrum.* **79**, 056102 (2008).
17. T. Irifune, F. Isobe, T. Shinmei, A novel large-volume Kawai-type apparatus and its application to the synthesis of sintered bodies of nano-polycrystalline diamond. *Phys. Earth Planet. In.* **228**, 255–261 (2014).
18. T. Sakai, T. Yagi, H. Ohfuji, T. Irifune, Y. Ohishi, N. Hirao, Y. Suzuki, Y. Kuroda, T. Asakawa, T. Kanemura, High-pressure generation using double stage micro-paired diamond anvils shaped by focused ion beam. *Rev. Sci. Instrum.* **86**, 033905 (2015).
19. S. S. Lobanov, V. B. Prakapenka, C. Prescher, Z. Konôpková, H.-P. Liermann, K. L. Crispin, C. Zhang, A. F. Goncharov, Pressure, stress, and strain distribution in the double-stage diamond anvil cell. *J. Appl. Phys.* **118**, 035905 (2015).
20. Y. K. Vohra, G. K. Samudrala, S. L. Moore, J. M. Montgomery, G. M. Tsoi, N. Velisavljevic, High pressure studies using two-stage diamond micro-anvils grown by chemical vapor deposition. *High Pressure Res.* **35**, 282–288 (2015).
21. N. A. Solopova, N. Dubrovinskaia, L. Dubrovinsky, Synthesis of nanocrystalline diamond from glassy carbon balls. *J. Cryst. Growth* **412**, 54–59 (2015).
22. I. Kantor, V. Prakapenka, A. Kantor, P. Dera, A. Kurnosov, S. Sinogeikin, N. Dubrovinskaia, L. Dubrovinsky, BX90: A new diamond anvil cell design for X-ray diffraction and optical measurements. *Rev. Sci. Instrum.* **83**, 125102 (2012).
23. N. Dubrovinskaia, L. Dubrovinsky, M. Hanfland, M. Hofmann, Diamond anvils with a spherical support designed for X-ray and neutron diffraction experiments in DAC. *High Pressure Res.* **32**, 537–543 (2012).
24. A. Snigirev, I. Snigireva, V. Kohn, S. Kuznetsov, I. Schelokov, On the possibilities of x-ray phase contrast microimaging by coherent high-energy synchrotron radiation. *Rev. Sci. Instrum.* **66**, 5486 (1995).
25. A. Snigirev, V. Kohn, I. Snigireva, B. Lengeler, A compound refractive lens for focusing high-energy X-rays. *Nature* **384**, 49–51 (1996).
26. Y. Akahama, H. Kawamura, Pressure calibration of diamond anvil Raman gauge to 410 GPa. *J. Phys. Conf. Ser.* **215**, 012195 (2010).
27. Y.-Y. Chang, S. D. Jacobsen, M. Kimura, T. Irifune, I. Ohno, Elastic properties of transparent nano-polycrystalline diamond measured by GHz-ultrasonic interferometry and resonant sphere methods. *Phys. Earth Planet In.* **228**, 47–55 (2014).
28. R. S. McWilliams, J. H. Eggert, D. G. Hicks, D. K. Bradley, P. M. Celliers, D. K. Spaulding, T. R. Boehly, G. W. Collins, R. Jeanloz, Strength effects in diamond under shock compression from 0.1 to 1 TPa. *Phys. Rev. B* **81**, 014111 (2010).
29. M. I. Eremets, I. A. Trojan, P. Gwaze, J. Huth, R. Boehler, V. D. Blank, The strength of diamond. *Appl. Phys. Lett.* **87**, 141902 (2005).
30. J.-J. Zhao, S. Scandolo, J. Kohanoff, G. L. Chiarotti, E. Tosatti, Elasticity and mechanical instabilities of diamond at megabar stresses: Implications for diamond-anvil-cell research. *Appl. Phys. Lett.* **75**, 487 (1999).
31. F. Cleri, P. Keblinski, L. Colombo, D. Wolf, S. R. Phillpot, On the electrical activity of sp^2 -bonded grain boundaries in nanocrystalline diamond. *Europhys. Lett.* **46**, 671–677 (1999).
32. J.-Y. Raty, G. Galli, C. Bostedt, T. W. van Buuren, L. J. Terminello, Quantum confinement and fullerenelike surface reconstructions in nanodiamonds. *Phys. Rev. Lett.* **90**, 037401 (2003).
33. M. Yokoo, N. Kawai, K. G. Nakamura, K.-i. Kondo, Y. Tange, T. Tsuchiya, Ultrahigh-pressure scales for gold and platinum at pressures up to 550 GPa. *Phys. Rev. B* **80**, 104114 (2009).
34. S. M. Dorfman, V. B. Prakapenka, Y. Meng, T. S. Duffy, Intercomparison of pressure standards (Au, Pt, Mo, MgO, NaCl and Ne) to 2.5 Mbar. *J. Geophys. Res.* **117**, B08210 (2012).
35. Y. Fei, A. Ricolleau, M. Frank, K. Mibe, G. Shen, V. Prakapenka, Toward an internally consistent pressure scale. *Proc. Natl. Acad. Sci. U.S.A.* **104**, 9182–9186 (2007).
36. K. Takemura, A. Dewaele, Isothermal equation of state for gold with a He-pressure medium. *Phys. Rev. B* **78**, 104119 (2008).
37. T. S. Duffy, G. Shen, J. Shu, H.-K. Mao, R. J. Hemley, A. K. Singh, Elasticity, shear strength, and equation of state of molybdenum and gold from x-ray diffraction under nonhydrostatic compression to 24 GPa. *J. Appl. Phys.* **86**, 6729 (1999).
38. H. Marquardt, S. Speziale, A. Gleason, S. Sinogeikin, I. Kantor, V. B. Prakapenka, Brillouin scattering and x-ray diffraction of solid argon to 65 GPa and 700 K: Shear strength of argon at HP/HT. *J. Appl. Phys.* **114**, 093517 (2013).
39. A. C. Larson, R. B. Von Dreele, "General structure analysis system (GSAS)" (Los Alamos National Laboratory Report LAUR 86–748, 2000).
40. B. H. Toby, *EXPGUI*, a graphical user interface for *GSAS*. *J. Appl. Crystallogr.* **34**, 210–213 (2001).
41. Y. Sun, J. Yuan, Electron energy loss spectroscopy of core-electron excitation in anisotropic systems: Magic angle, magic orientation, and dichroism. *Phys. Rev. B* **71**, 125109 (2005).

Acknowledgments: We thank T. Irifune for providing us with samples of NPD used here. N.D. and L.D. thank K. Doubrovinski for useful discussions of elasticity theory. We also gratefully acknowledge the assistance of C. Detlefs, P. Wattecamps, and M. Lubomirsky (ESRF); M. Süpfle (ANKA); and M. Polikarpov and I. Lyatun (Immanuel Kant Baltic Federal University). We acknowledge the Synchrotron Light Source ANKA for provision of instruments at the IR2 beamline. **Funding:** N.D. thanks the German Research Foundation [Deutsche Forschungsgemeinschaft (DFG)] and the Federal Ministry of Education and Research (BMBF; Germany) for financial support through the DFG Heisenberg Programme (projects no. DU 954-6/1 and DU 954-6/2) and project no. DU 954-8/1 and the BMBF grant no. 5K13WC3 (Verbundprojekt O5K2013, Teilprojekt 2, PT-DESY). L.D. thanks the DFG and the BMBF (Germany) for financial support. Portions of this work were performed at GSECARS (Sector 13), APS, Argonne National Laboratory. GSECARS is supported by the NSF Earth Sciences (EAR-1128799) and the U.S. Department of Energy (DOE) GeoSciences (DE-FG02-94ER14466). This research used resources of the APS, a DOE Office of Science user facility operated for the DOE Office of Science by Argonne National Laboratory under contract no. DE-AC02-06CH11357. A.S. thanks the Ministry of Science and Education of Russian Federation through grant no. 14.Y26.31.0002 for financial support. **Author contributions:** L.D. and N.D. conceptualized, planned, coordinated the study, conducted all DAC experiments, analyzed the data, and wrote the paper; N.A.S. and N.D. synthesized the NCD balls; L.D., N.D., M.H., E.B., M.B., C.P., and V.B.P. conducted synchrotron x-ray diffraction experiments at ultrahigh pressures; A.A. and S.T. performed the TEM analysis; I.C., B.G., Y.-L.M., L.D., and N.D. performed IR spectroscopy experiments; S.P. milled NCD balls using the FIB technique; and P.E., I.S., and A.S. conducted synchrotron x-ray microscopy experiments. All authors discussed the results and commented on the paper. **Competing interests:** The authors declare that they have no competing interests. **Data and materials availability:** All data needed to evaluate the conclusions in the paper are present in the paper and/or the Supplementary Materials. Additional data related to this paper may be requested from the authors.

Submitted 17 February 2016
Accepted 24 June 2016
Published 20 July 2016
10.1126/sciadv.1600341

Citation: N. Dubrovinskaia, L. Dubrovinsky, N. A. Solopova, A. Abakumov, S. Turner, M. Hanfland, E. Bykova, M. Bykov, C. Prescher, V. B. Prakapenka, S. Petitgirard, I. Chuvashova, B. Gasharova, Y.-L. Mathis, P. Ershov, I. Snigireva, A. Snigirev, Terapascal static pressure generation with ultrahigh yield strength nanodiamond. *Sci. Adv.* **2**, e1600341 (2016).

ScienceAdvances
AAAS

Terapascal static pressure generation with ultrahigh yield strength nanodiamond

Natalia Dubrovinskaia, Leonid Dubrovinsky, Natalia A. Solopova, Artem Abakumov, Stuart Turner, Michael Hanfland, Elena Bykova, Maxim Bykov, Clemens Prescher, Vitali B. Prakapenka, Sylvain Petitgirard, Irina Chuvashova, Biliana Gasharova, Yves-Laurent Mathis, Petr Ershov, Irina Snigireva and Anatoly Snigirev (July 20, 2016)

Sci Adv 2016, 2:.
doi: 10.1126/sciadv.1600341